



# Validation of Hydrodynamic Load Models Using CFD for the OC4-DeepCwind Semisubmersible

## Preprint

M.A. Benitz, D.P. Schmidt, M.A. Lackner,  
and G.M. Stewart  
*University of Massachusetts*

J. Jonkman and A. Robertson  
*National Renewable Energy Laboratory*

*To be presented at the ASME 2015 International Conference on  
Ocean, Offshore and Arctic Engineering  
St. John's, Newfoundland, Canada  
May 31 – June 5, 2015*

**NREL is a national laboratory of the U.S. Department of Energy  
Office of Energy Efficiency & Renewable Energy  
Operated by the Alliance for Sustainable Energy, LLC**

This report is available at no cost from the National Renewable Energy Laboratory (NREL) at [www.nrel.gov/publications](http://www.nrel.gov/publications).

**Conference Paper**  
NREL/CP-5000-63751  
March 2015

Contract No. DE-AC36-08GO28308

## NOTICE

The submitted manuscript has been offered by an employee of the Alliance for Sustainable Energy, LLC (Alliance), a contractor of the US Government under Contract No. DE-AC36-08GO28308. Accordingly, the US Government and Alliance retain a nonexclusive royalty-free license to publish or reproduce the published form of this contribution, or allow others to do so, for US Government purposes.

This report was prepared as an account of work sponsored by an agency of the United States government. Neither the United States government nor any agency thereof, nor any of their employees, makes any warranty, express or implied, or assumes any legal liability or responsibility for the accuracy, completeness, or usefulness of any information, apparatus, product, or process disclosed, or represents that its use would not infringe privately owned rights. Reference herein to any specific commercial product, process, or service by trade name, trademark, manufacturer, or otherwise does not necessarily constitute or imply its endorsement, recommendation, or favoring by the United States government or any agency thereof. The views and opinions of authors expressed herein do not necessarily state or reflect those of the United States government or any agency thereof.

This report is available at no cost from the National Renewable Energy Laboratory (NREL) at [www.nrel.gov/publications](http://www.nrel.gov/publications).

Available electronically at <http://www.osti.gov/scitech>

Available for a processing fee to U.S. Department of Energy and its contractors, in paper, from:

U.S. Department of Energy  
Office of Scientific and Technical Information  
P.O. Box 62  
Oak Ridge, TN 37831-0062  
phone: 865.576.8401  
fax: 865.576.5728  
email: <mailto:reports@adonis.osti.gov>

Available for sale to the public, in paper, from:

U.S. Department of Commerce  
National Technical Information Service  
5285 Port Royal Road  
Springfield, VA 22161  
phone: 800.553.6847  
fax: 703.605.6900  
email: [orders@ntis.fedworld.gov](mailto:orders@ntis.fedworld.gov)  
online ordering: <http://www.ntis.gov/help/ordermethods.aspx>

*Cover Photos: (left to right) photo by Pat Corkery, NREL 16416, photo from SunEdison, NREL 17423, photo by Pat Corkery, NREL 16560, photo by Dennis Schroeder, NREL 17613, photo by Dean Armstrong, NREL 17436, photo by Pat Corkery, NREL 17721.*

# VALIDATION OF HYDRODYNAMIC LOAD MODELS USING CFD FOR THE OC4-DEEPCWIND SEMISUBMERSIBLE

**Maija A. Benitz  
David P. Schmidt  
Matthew A. Lackner  
Gordon M. Stewart**

Department of Mechanical and Industrial Engineering  
160 Governor's Drive  
University of Massachusetts  
Amherst, Massachusetts 01003  
Email: mbenitz@engin.umass.edu

**Jason Jonkman  
Amy Robertson**

National Renewable Energy Laboratory  
15013 Denver W Pkwy  
Golden, Colorado USA 80401

## ABSTRACT

*Computational fluid dynamics (CFD) simulations were carried out on the OC4-DeepCwind semisubmersible to obtain a better understanding of how to set hydrodynamic coefficients for the structure when using an engineering tool such as FAST to model the system. This study focussed on the drag behavior and the effects of the free surface, free ends and multimember arrangement of the semisubmersible structure. These effects are investigated through code-to-code comparisons and flow visualizations. The implications on mean load predictions from engineering tools are addressed. This study suggests that a variety of geometric factors should be considered when selecting drag coefficients. Furthermore, CFD simulations demonstrate large time-varying loads caused by vortex shedding that FAST's hydrodynamic module, HydroDyn, does not model. The implications of these oscillatory loads on the fatigue life needs to be addressed.*

## INTRODUCTION

Engineering tools for predicting loads on offshore floating wind turbine platforms often rely on a combination of potential-flow theory for radiation and diffraction effects and strip theory (through Morison's equation) for viscous-drag effects. For Morison's equation to perform most accurately, selecting appropriate drag coefficients is imperative. A common method for se-

lecting drag coefficients for engineering tools is based on the Reynolds number from experimental data for fully submerged, infinite cylinders. However, a semisubmersible has finite draft, pierces the free surface, and has an array of cylinders, so the infinite cylinder drag coefficient may not apply. Because of these geometric differences, assuming the drag coefficient is a function of only the Reynolds number may not be appropriate. Further investigation of drag on individual members of the semisubmersible is warranted to prescribe the most appropriate drag coefficient and verify inertial load predictions in the engineering models.

To investigate the influences of the complex geometry on the choice of drag coefficient, computational fluid dynamics (CFD) simulations were performed. CFD models in OpenFOAM were validated previously by comparing numerical drag predictions on cylinders to experimental work at various Reynolds numbers. This validation exercise provided great confidence in using the CFD models for the simulations performed for this study. Next, a code-to-code comparison was carried out between HydroDyn [1], the hydrodynamics module of FAST, a wind turbine tool developed by the National Renewable Energy Laboratory (NREL) for employing engineering models [2], and OpenFOAM. Global load predictions from OpenFOAM and HydroDyn were presented at OMAE 2014 by Benitz, et al [3], for the Offshore Code Comparison Collaboration Continuation (OC4)

DeepCwind semisubmersible analyzed in the International Energy Agency (IEA) Wind Task 30 project [4] as a first step towards validation of the engineering tool.

This study presents loads on individual members of the semisubmersible and highlights the effects of shadowing, interaction between structure members, and the importance of carefully selecting drag coefficients for engineering models. This work focused only on drag because the previous work successfully validated the radiation/diffraction solution of the potential-flow solution through comparison of wave-loading simulations in HydroDyn and OpenFOAM. This study followed that previous work, trying to understand why OpenFOAM did not match HydroDyn well for the current-only case, where drag is important, and the key features that cause these loads to differ from those seen for submerged, infinite cylinders. Drag effects are also important in severe sea states.

It was hypothesized that discrepancies in load predictions from the previous work could be due to a variety of factors, including shadowing effects, treatment of interaction between individual members, or even the selection, or prediction, of drag coefficients. In each of the OpenFOAM simulations discussed in the previous work, the geometry considered was treated as a single patch, meaning each simulation produced only one global force prediction.

For this study, loads on separate structural members were investigated to better understand the significance of shadowing and interactions between members, as well as the influence of a free surface and free ends. CFD is used to examine the influence of a complex geometry on the drag of a structure as compared to the experimental measurements for submerged, infinite cylinders. Insight about the role of shadowing is provided through CFD force predictions and flow visualizations. The roles of the free surface, free ends, and wake effects are discussed in terms of inertial and drag loads on the semisubmersible. The implications of these factors on loading predictions in engineering tools are addressed with regard to modeling assumptions and approximations in HydroDyn and other similar codes.

In addition to assessing the mean drag predictions on the semisubmersible, the CFD solution can also quantify the importance of the transient loads induced by vortex shedding. Time histories of the load predictions in the inline and transverse directions, as computed with CFD, provide information about the magnitude and frequency of the oscillatory loads. These time varying loads merit further attention because of their potential fatigue impacts and absence in Morison-based engineering models.

This work serves to better inform those that use engineering tools when selecting drag coefficients for offshore structures that differ from infinitely long, fully submerged cylinders. It demonstrates that careful selection of coefficients as inputs to computer-aided engineering (CAE) tools is necessary and important. CFD simulations presented here provide improved understanding of

the drag behavior of more complex structures, and this knowledge can be extended to engineering models, such as HydroDyn.

### Geometric Factors Affecting the Drag

Often, the drag coefficient input to HydroDyn, and other similar engineering tools, is chosen based on the Reynolds number alone. Moreover, the drag coefficient is often determined based on previous experimental work on fully submerged, infinitely long cylinders. The semisubmersible components are neither infinitely long nor fully submerged, and it was hypothesized that these factors alter the drag coefficient, which is discussed later in this paper.

In fact, previous work from the literature demonstrates that the drag coefficient on a circular cylinder can be sensitive to many factors, including the presence of a free surface, and a free end of a body. In addition, the presence of multiple members will disrupt the flow such that the drag characteristics will be altered as well. If tools are not capable of modeling this disturbed flow, the parameters must be used to approximate this influence. Insight is gained from a review of previous work that has investigated these individual factors on cylinders. Furthermore, the results provided confidence in the drag coefficient predictions from CFD in this study where multiple factors were combined. Indeed, these factors do alter the drag behavior on the semisubmersible in the current conditions considered here, as discussed below.

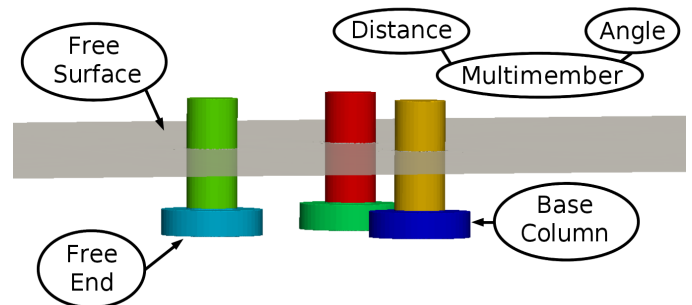


**FIGURE 1.** Contributions to the drag coefficient of the semisubmersible platform for offshore wind turbines.

Various authors have examined the effects of a free surface on the drag behavior of vertical cylinders. In all of these works, vertical cylinders that pierce the free surface of an air-water interface were studied. Experimental work by Chaplin and Teigen [5] demonstrated that the drag coefficient decreases near the free surface of the water. Numerical work by Yu [6], Kawamura [7] and Suh [8] found drag coefficients that were smaller than the drag coefficient for fully submerged cylinders in the same flow conditions. There is numerical and experimental evidence that the

presence of a free surface decreases the drag coefficient on vertical cylinders.

The role of free ends has also been investigated numerically and experimentally. Experimental studies by Sumner [9] demonstrated reduced drag coefficients for cylinders with a free end about which the flow could accelerate. Sumner’s work investigated drag in uniform flow conditions, but the same effects were found in waves. Niedzwecki [10] performed experiments on truncated cylinders in regular and random waves and found that the normalized drag on truncated cylinders was lesser than that on infinitely long cylinders.

Drag behavior on bodies consisting of multiple members has also been investigated. Sumner provides a thorough review of dual-cylinder configurations [11]. For cylinders placed in a tandem configuration, in which one cylinder is directly upstream of the other, it was found that the upstream cylinder has a lower drag coefficient than it would if the cylinder were isolated. Furthermore, at certain distances, the downstream cylinder can experience a negative drag. When cylinders were arranged side-by-side, a certain spacing existed where the drag reached a minimum. Finally, when the cylinders were staggered, certain angles and spacings existed in which drag minima are seen. In all of these scenarios, the wake behind the first cylinder alters the flow field such that the drag behavior is different from that of an isolated cylinder.

Overall, the effects of a free surface, free end, and multi-body configuration are shown to cause a decrease in drag coefficient on a vertical cylinder. There is reason to believe that these same factors are the causes for decreases in the drag coefficient of many members of the semisubmersible structure as well—such as the upper, base, and main columns, which are shown in a later section. This study examines the combined effects of the free surface, free end, and multi-body configuration of the semisubmersible on the drag behavior.

## ANALYSIS SPECIFICATIONS

The OC4-DeepCwind semisubmersible structure was used in this study. This geometry was studied in previous work [3] and will be used for future studies of motion in waves and current with comparisons to experimental data from DeepCwind [12]. However, instead of modeling the entire geometry, only the three offset columns were investigated in this work. The simplified geometry should provide more general findings about the drag coefficient, which can be extended to other similar proposed geometries in the offshore ocean engineering community. Furthermore, previous work comparing predictions from HydroDyn and OpenFOAM demonstrated more accurate drag predictions for smaller members than larger members, as is expected from Morison’s equation.

The specifications of the semisubmersible platform are presented in Table 1. CFD simulations are performed at 1/50th the

scale of the prototype semisubmersible platform. The dimensions used in the CFD simulations match the dimensions of the scale model tested in the Maritime Research Institute Netherlands (MARIN) wave tank [12]. Results are presented at prototype scale, scaled from model scale with Froude scaling relationships. CFD simulations are performed at the model scale because of the lesser demand on mesh cell count, as well as the high confidence of the model’s performance at model-scale Reynolds numbers.

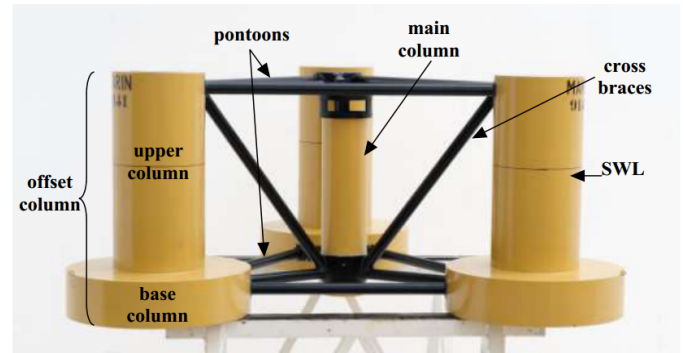


**FIGURE 2.** The semisubmersible built to model scale, at 1/50 of the prototype size, for the DeepCwind tank tests. [4]

The 1/50 scale model of the semisubmersible platform built for the DeepCwind tank testing campaign is shown in Figure 2. The geometry consists of three larger offset columns, which include an upper column and a larger diameter base column. A central column, called the main column, is connected to the offset columns with pontoons and cross braces (which are not modeled in this study). This work omits treatment of the wind turbine and therefore, does not discuss the tower and turbine properties.

In the simulations, the semisubmersible platform is oriented such that one column is located in front and centered, and the other two columns are downstream and parallel to one another. The column that is upstream of the others is called the front column, and the two downstream columns are called the right and left columns, according to their position relative to the front column when looking in the direction of the current flow.

Simulations were carried out in current-only conditions, at a uniform velocity of 0.085 m/s, at model scale. This corresponds to a current velocity of 0.6 m/s at prototype scale. Additionally, simulations were performed with HydroDyn, using the same environmental conditions and semisubmersible orientation as the CFD simulations. The results from the two codes are presented for comparison in Section 4. These flow conditions correspond to Froude number of 0.055, where  $Fr = \frac{U}{\sqrt{gL}}$ . The Reynolds numbers are given in Table 2.

**TABLE 1.** Specifications of the semisubmersible structural components [4]

Platform draft	20.0 m
Centerline spacing between offset columns	50.0 m
Length of upper columns	26.0 m
Length of base columns	6.0 m
Diameter of main column	6.5 m
Diameter of offset (upper) columns	12.0 m
Diameter of base columns	24.0 m
Diameter of pontoons and cross braces	1.6 m

**TABLE 2.** The Reynolds numbers of the upper and base columns, at both model and prototype scale. The Froude number is 0.055 at both scales.

	Model Scale Re	Prototype Scale Re
Upper Column	20,361	7,200,000
Base Column	40,704	14,400,000

## METHODS

### FAST

FAST is an aero-hydro-servo-elastic engineering tool used for simulating wind turbines. FAST (version 8) uses a modularized framework, where the HydroDyn module includes all the hydrodynamics modeling. HydroDyn allows for the development of a hybrid model based on strip and potential-flow theories. WAMIT, a potential-flow-based panel method, is used as a preprocessor for input to HydroDyn. Strip theory is applied with the viscous drag term from Morison’s equation [1].

The radiation and diffraction problems were neglected in this work, as the body is fixed in space, and furthermore there were no incident waves because of the current-only environmental conditions. As such, potential-flow solutions were not included in the load predictions in this work. Instead, the load predictions were provided entirely from strip theory, through Morison’s equation.

In its full form, Morison’s equation includes a term for inertia-induced wave excitation loads (with a long wavelength approximation), radiation induced added mass, and viscous drag loads. Again, radiation and diffraction effects are neglected in this work because the platform is fixed, no waves are present, and the current is steady. Therefore, the viscous drag term is the only contribution to the overall load on the platform. Each platform member is assigned a unique drag coefficient based on

the Reynolds number associated with specific member geometry and current condition. The viscous load predictions are provided as a force per unit length for several nodes along the length of the member. The load predictions are then integrated along the length of each segment, and the results are summed to provide a total load on the member. The effects of interactions between members is neglected in this formulation.

This research uses a FAST 8 model of the semisubmersible created for use in the OC4 program [4]. The hydrodynamic model has been additionally modified to include only the upper and lower offset columns (no pontoons, cross braces, or main column). The platform was fixed in space by turning off all structural degrees of freedom and enabling only the hydrodynamic force calculation. The model has no wind or wave inputs, instead, a current of 0.6 m/s is applied (but using model-scale Re). In this way, the FAST model operates similarly to the CFD model described in the following section.

### OpenFOAM

CFD simulations are carried out with the opensource software package OpenFOAM, described by Weller, et al [13]. Numerical simulations are performed using the incompressible Navier-Stokes equations, which are derived from the first principles of conservation of mass and momentum. The continuous partial differential equations are recast into a system of linear equations. Problem closure to the Navier-Stokes equation is provided with a Newtonian relationship between stress and strain. A PISO-SIMPLE (PIMPLE) algorithm is used for solving the pressure-velocity coupling. The linear equations are solved using a geometric-algebraic multigrid method (GAMG) method.

The multiphase flow of air and water is modeled with the volume-of-fluid (VOF) method. The VOF method models two-phase flows with a dimensionless scalar field representing the fluid volume fraction. A volume fraction value of zero represents fluid “a,” and a value of one represents fluid “b.” The volume fraction is advected with the flow via a transport equation. The transport equation is solved simultaneously with the equations of mass and momentum conservation. The VOF method was first introduced and developed by Noh and Woodward [14], Hirt and Nichols [15], and deBar [16].

The indicator function,  $\alpha$ , is given by [17],

$$\alpha = \begin{cases} 0 & \text{for a point inside fluid “a”} \\ 0 < \alpha < 1 & \text{for a point inside transitional region} \\ 1 & \text{for a point inside fluid “b”} \end{cases} \quad (1)$$

The indicator function, or fluid volume fraction, is advected with the flow. Because issues can arise when convecting a step function due to numerical diffusion, an artificial compression term can be used to compress the interface. This term was first proposed by Weller (and presented by Rusche) [17], and is presented

in the third term of the transport equation below,

$$\frac{\partial \alpha}{\partial t} + \nabla \cdot (\mathbf{U}\alpha) + \nabla \cdot (\mathbf{U}_r\alpha(1 - \alpha)) = 0. \quad (2)$$

The CFD models used in this work have been thoroughly validated against a variety of experimental data. The validation exercises were documented in previous work [3]. The DeepCwind tank tests did not include current tests from which we could have validated the specific model applied in this study [12].

The Spalart-Allmaras one-equation model [18] is used to model turbulence. A Spalding wall function is applied at the cylinder wall [19]. The turbulence model was selected based on validation exercises described in the previous work [3], which are briefly outlined here. In the previous work, uniform flow past a fully-submerged cylinder was simulated with OpenFOAM. A variety of turbulence models were tested in the previous work, and the Spalart-Allmaras turbulence model gave results that matched best with experimental data. Furthermore, simulations with Spalart-Allmaras did not result in excessive damping of vortices in the wake as was seen with both versions of the k-Epsilon models. A sensitivity study was also carried out to examine the effects of initial conditions of the Spalart-Allmaras model. Additionally, a mesh convergence study was carried out to determine the meshing requirements for a cylinder in uniform flow.

Numerical meshes were generated with increased mesh refinement near the surface of the semisubmersible body and also around the fluid interface. Three unstructured meshes were generated, with 1.94, 2.88, and 5.06 million cells each. Sensitivity of the model to grid density was again tested for the computational meshes used in this study. The results of this mesh convergence study are given in Figure 3. It was found that the inline force predictions show convergence after a mesh size of 2.88 million cells. A  $y+$  value of 61 was used on the surface of the columns, which is appropriate given the use of the Spalding wall function. A vertical slice through the coarsest numerical domain is presented in Figure 4. The entire numerical domain is illustrated in Figure 5.

The offset columns, in the absence of the main column, pontoons, and cross braces, of the geometry were selected for further investigation because of their more simplistic form. The absence of cross braces and pontoons reduces the complexity of the flow, allowing for better understanding of the fundamental flow behavior. Numerical meshes were generated for CFD simulations consisting of only the three offset columns. The results presented in the Loads on Individual Offset Columns section used a mesh with three isolated surface patches, while the results in the Loads on Upper and Base Columns section are from a mesh with six surface patches.

The bottom and sides of the domain are prescribed as no-slip boundaries conditions on velocity. The pressure and volume fraction are zero-gradient at the walls and the floor. An

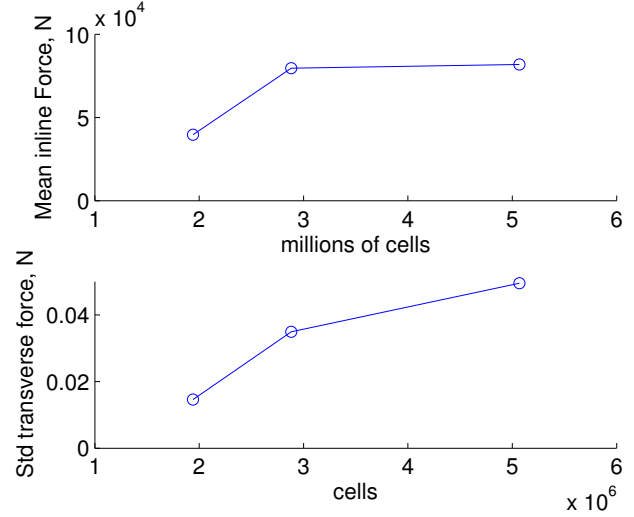


**FIGURE 3.** Mesh convergence results for the mean inline force and the standard deviation of the transverse force, in the top and bottom plots, respectively.

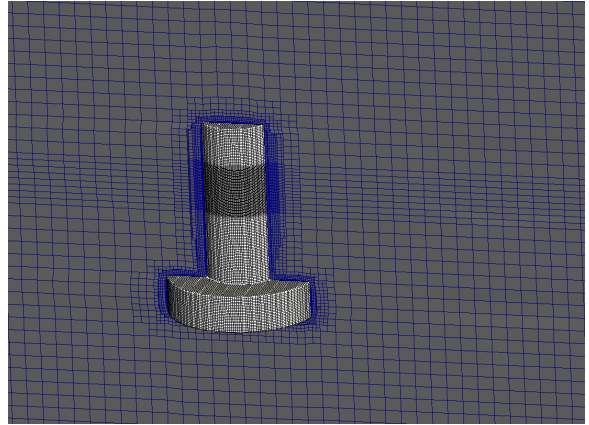


**FIGURE 4.** Vertical slice through the domain to illustrate the increased level of mesh refinement around the free surface, as well as the refinement surrounding the body.

atmospheric boundary condition is used for the top, in which the pressure changes with velocity, as prescribed by the *totalPressure* condition in OpenFOAM. A uniform velocity is prescribed in the water phase at the inlet. The volume fraction is given as 1 below the still water line (SWL) and 0 above, where 1 represents water and 0 is air. The internal domain is initialized with a zero-velocity flow field.

The maximum Courant number ( $Co = U \frac{\Delta t}{\Delta x}$ , where  $U$  is the velocity and  $\Delta t$ ,  $\Delta x$  are the discretized time and length intervals) was set to 0.5. An initial time step of 0.01s was given, and the timestep was adjusted automatically according to the Courant

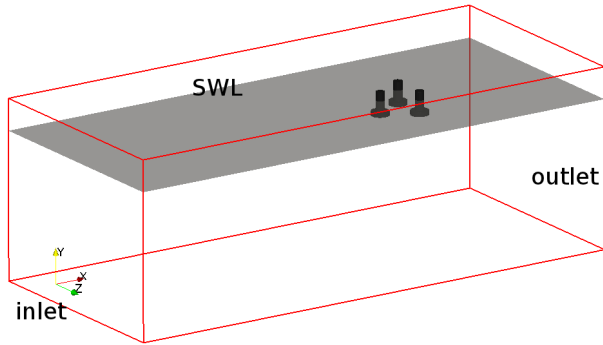


**FIGURE 5.** Computational domain for the simplified OC4-DeepCwind semisubmersible in uniform flow.

number through the simulation.

The predicted loads on the semisubmersible platform are computed by discrete integration of the pressure and viscous forces along the surface of the body. The total pressure and viscous forces are computed by summing the pressures and viscous forces on each face on the surface of the semisubmersible geometry. The total forces are given in three-component vectors in the  $x$ ,  $y$ , and  $z$ -directions.

## RESULTS AND DISCUSSION

CFD simulation results are presented for the simplified OC4-DeepCwind semisubmersible in current-only conditions. Results are first presented to compare load predictions between the three offset columns. Then the loading is discussed in further detail by examining differences in loads between the upper and base components of the offset columns. The trends in drag loads are presented quantitatively in the first two sub-sections. Next, the quantitative findings in the drag behavior are explained through various flow visualizations. Finally, mean inline force predictions from HydroDyn are presented, with the drag coefficients determined from CFD at three current velocities.

### Loads on Individual Offset Columns

The CFD results for the inline and transverse forces on each of the individual offset columns are shown in Figure 6. The results are shown between 250 s and 350 s, once the initial transients, due to the quiescent initial conditions on velocity, of the simulation have subsided. The top plot shows the inline force predictions on the front, right and left columns. A lag in the peaks of the forces can be seen in the right, and left column loads, as compared to the front column. The bottom plot displays the transverse force predictions on the three columns. The magnitude of the transverse forces on the right and left columns is greater than on the front column, which is likely a result of flow diffraction and vortex shedding on the downstream columns.

Furthermore, it is interesting to note that the transverse forces on the two downstream columns are completely out of phase with each other, indicating symmetrical vortex shedding off of the trailing columns.

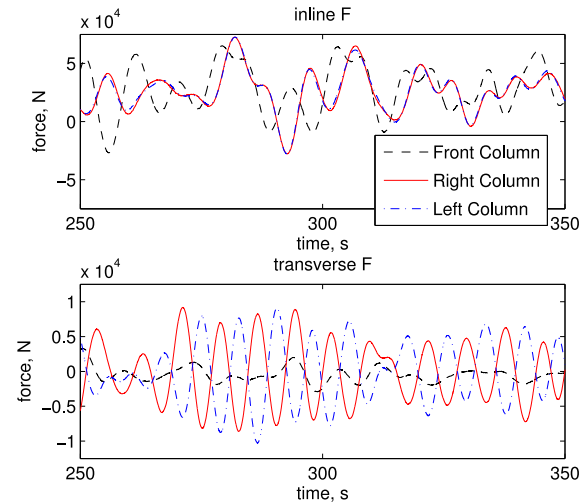


**FIGURE 6.** Inline and transverse force predictions from OpenFOAM. The load predictions are shown in black, red, and blue for the front, right, and left columns, respectively.

To investigate the inline force predictions further, the mean force predictions on each column, from OpenFOAM, are calculated. These mean inline forces are shown in the first three bars of Figure 7. The red error bars indicate one standard deviation from the mean, to illustrate the degree to which the periodic force signal oscillates about the mean. The bar on the far right of Figure 7 shows the inline force prediction from HydroDyn. HydroDyn calculates the inline force as a mean value, without any time-varying oscillation, so the standard deviation of the signal is zero. The bar labeled  $C_d = 1.0$  shows the result from a HydroDyn simulation where the base and upper columns are each assigned a drag coefficient equal to one. The drag coefficient of 1.0 corresponds to the model-scale Reynolds numbers of the upper and base columns. These drag coefficients for input to HydroDyn are selected from a straightforward Reynolds number versus drag coefficient curve. Without consideration of the free surface, free end or multimember effects, it was expected that a drag coefficient equal to 1.0 would be most appropriate for the model-scale simulations carried out in this work, but that was not found to be true in practice.

The mean inline force predictions from OpenFOAM are very similar for each of the three offset columns, and not surprisingly, are in near perfect agreement for the two downstream

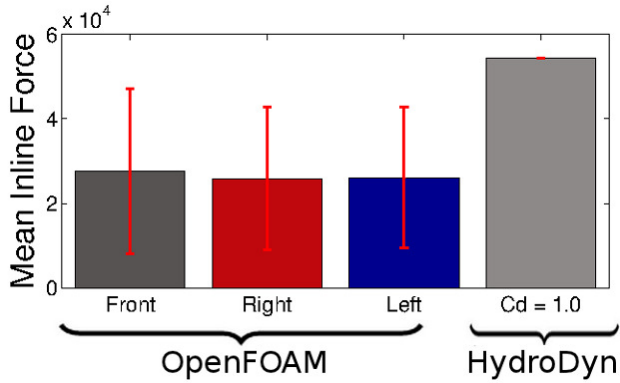


**FIGURE 7.** Mean inline force predictions from OpenFOAM and HydroDyn. The three bars on the left show the results from OpenFOAM. The bar on the right shows predictions from HydroDyn, for the inline force on a single column. Error bars indicate one standard deviation in the time-varying force signals from OpenFOAM.

columns. The agreement between HydroDyn and OpenFOAM is not very good when the drag coefficients are set to 1.0.

These findings illustrate three main points. First, the OpenFOAM results seem to indicate that shadowing effects do not play a major role in the loading on the structure, as demonstrated by the very similar inline forces on the front, right, and left columns. However, this finding will be questioned in the next subsection when loads on individual members are investigated. Second, these results point to the pivotal role the drag coefficient plays in loading predictions in current-only conditions. It is possible that OpenFOAM is underpredicting the drag on the body; however, prior validation work showed great accuracy in the drag prediction in this Reynolds number range. The drag coefficient selection in HydroDyn could be at fault. It may be too simplistic to select the drag coefficient from a simple Reynolds number relationship, especially one that is based on an infinitely long, fully submerged cylinder. Third, the time variation of load is the result of vortex shedding, not modelled by the viscous drag term from Morison's equation.

### Loads on Upper and Base Columns

To further investigate the inline forces on the offset columns of the semisubmersible column, the loads on the upper and base columns of the front and trailing offset columns are examined individually. Whereas the results in the previous section would indicate roughly uniform loading on each offset column, the results here show that loading varies greatly depending on upstream versus downstream location, as well at proximity to the free surface. While these results are for a specific geometry in a single flow condition, we hypothesize that these factors will affect loads on other geometries in similar flow conditions, such that careful at-

tention must be given to selecting input parameters to engineering tools.

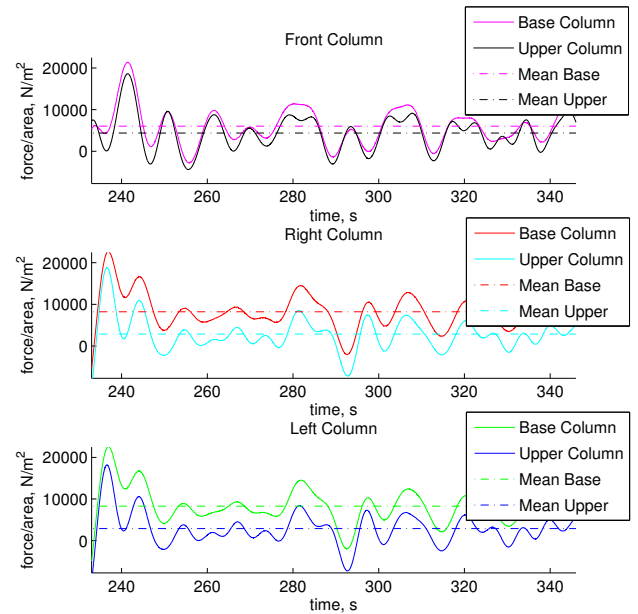


**FIGURE 8.** Forces per unit area on the front, right, and left columns are shown in the top, middle, and bottom plot, respectively in a current of 0.6 m/s. Solid lines show the time varying loads, and the dash-dot lines show the mean value used for computing the drag coefficient.

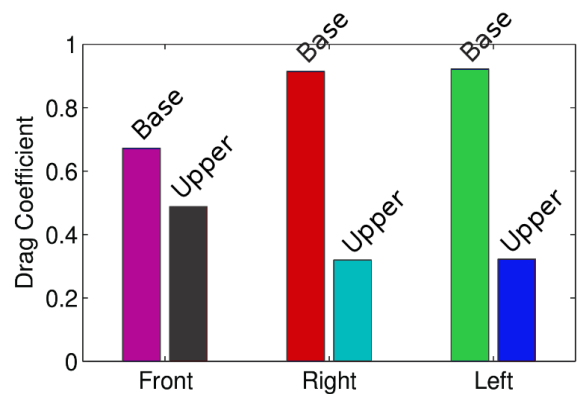


**FIGURE 9.** Predicted drag coefficients from an OpenFOAM simulation of the three offset columns in a current flow of  $U = 0.6$  m/s at prototype scale. The results for the base columns are shown in blue, and the upper columns are represented in red. The mean inline forces are illustrated with the dashed lines.

Again, simulations in OpenFOAM were carried out in current-only conditions with a uniform velocity equal to 0.085 m/s at model scale, corresponding to 0.6 m/s at prototype scale. The force predictions, per unit area, are presented in Figure 8. The forces per unit area on the front, right, and left columns are shown in the top, middle, and bottom plot, respectively. The magenta, red, and green lines show the loads per unit area on the base columns, and the black, cyan, and blue lines illustrate loads per unit area on the upper columns. Solid lines show the time varying loads, while the dash-dot lines show the calculated mean load. The loads per unit area on the base and upper columns are very similar for the front column. The downstream columns, however, give different loads per unit area for the base and upper columns. This indicates that the wake behind the front column is somehow affecting the loading on the body in a way that varies vertically.

The variation in loads between the upstream and downstream columns is not accounted for in HydroDyn where there is no model for shadowing of members, such that equal loads are predicted on each column. Additionally, the load predictions from HydroDyn do not vary in the vertical direction when modeling current-only conditions. Finally, HydroDyn does not compute time-varying loads for the current-only conditions, despite the fact that vortex shedding does occur in this flow regime.

The predicted drag coefficients from OpenFOAM are calculated for the base and upper columns for each of the three offset columns, based on the upstream undisturbed velocity. The results are presented in Figure 9. At the Reynolds number simulated here, the drag coefficient versus Reynolds curve for an infinitely long, fully submerged cylinder indicates that the drag coefficient should be roughly 1.0. The predicted drag coefficients from OpenFOAM are all below 1.0. The drag on the base columns increases for downstream members, while the drag on the upper columns decreases. These initially surprising results merit further investigation through flow visualization. The findings from flow visualization, and a brief survey of the literature discussed earlier, reveals that these predictions from OpenFOAM are likely correct. The following subsection provides and discusses flow field visualizations.

### Flow Visualizations

Here, visualizations of the velocity and pressure fields are presented to provide insight about the drag coefficients discussed above. The values in this section are presented at model scale—the scale at which the CFD simulations were performed. Additionally, the visualizations presented here are instantaneous values and have not been time averaged. These visualizations will highlight a variety of factors that may contribute to smaller predictions in the drag coefficient than previously anticipated. These factors include the presence of a free surface, free end effects of the body, and the multimember structure. As discussed earlier,

the literature suggests that each of these factors can lead to decreases in the drag behavior on the semisubmersible structure.

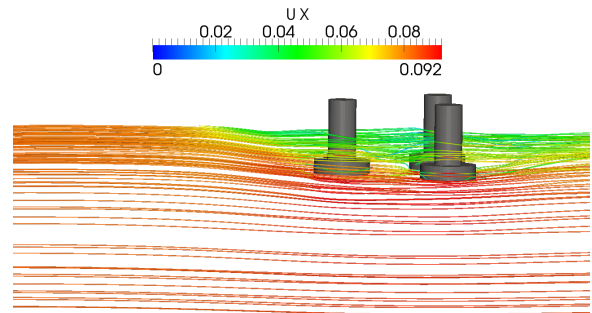


**FIGURE 10.** A side view of the streamlines where the flow travels from left to right. The flow slows as it approaches the body and near the free surface. Acceleration of the flow can be seen as the streamlines pass under the body.

A side view of the streamlines around the offset columns in current-only conditions is shown in Figure 10 where the flow moves from left to right. This visualization highlights the velocity drop near the body, and furthermore, near the free surface. Additionally, the flow is shown to accelerate as it passes under the geometry. Finally, the velocity near the free surface is further reduced after passing the front column, just before it reaches the two trailing columns. This single image highlights that the free surface, free ends, and multimember arrangement all appear to alter the drag behavior of the semisubmersible, as compared to that of an infinite cylinder.

Streamlines that are seeded nearer to the free surface are shown in Figure 11. They provide a better visualization of the vortex shedding in the wakes of the three offset columns. Again, reductions in the velocity in the current direction are seen near the free surface as the flow approached the body. Also, the effects of the multibody arrangement are illustrated in the increasing reduction in flow velocity behind the front column and before the trailing columns.

Horizontal slices at increasing depths—0.1, 0.2 and 0.3 m below the still water line (SWL)—are shown in Figure 12. The velocity magnitude is presented at three depths of submergence, where the magnitude increases with increasing depth. This reiterates the trend shown in Figure 10 where the flow is seen to slow near the free surface. The reduction in fluid velocity near the free surface where the body sits explains the reduced drag coefficient on the upper columns, as compared to the base columns that see a higher flow velocity. Again, the presence of the free surface is shown to affect the flow field near the structure.

Next, velocity vectors at the three depths—again, at 0.1, 0.2,

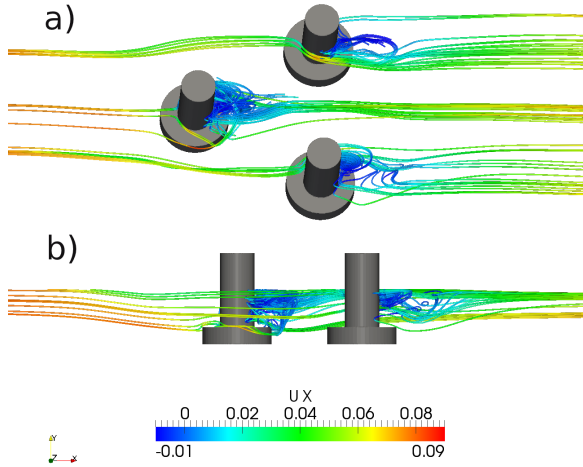


**FIGURE 11.** a) Bird's eye view of the streamlines past the simplified semisubmersible geometry, in a 0.085 m/s current flow traveling from left to right, at model scale. b) A side view of the streamlines.

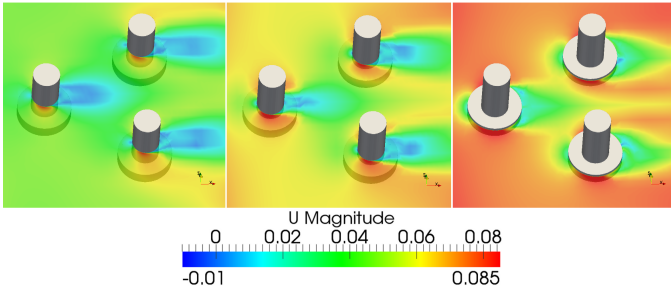


**FIGURE 12.** The velocity magnitude at three horizontal planes, located at 0.1, 0.2, and 0.3 m below the SWL, from left to right, shown at 42 s. The current direction is from left to right. The increasing velocity with increasing water depth highlights the role of the free surface in the fluid flow near the structure.

and 0.3 m below the SWL—are shown in Figure 13, from top to bottom, respectively. Again, a reduced velocity is seen near the free surface near the structure. With increasing water depth, the velocity increases. This image sheds light onto the effects of the multibody arrangement by illustrating the vector magnitudes and directions as they come off of each offset column. Perhaps most notable is the large magnitude velocities that point downwards from the front column onto the trailing base columns. These velocity vectors help to explain the increase in the drag on the trailing base columns.

Largely, the total pressure field is dominated by hydrostatics. To investigate local changes in the pressure, the hydrostatic component is subtracted from the total pressure, leaving a modified pressure term,  $\tilde{p}$ , that is  $p$  without  $\rho gz$ . This is described mathematically below, where  $p$  is defined as the total pressure,

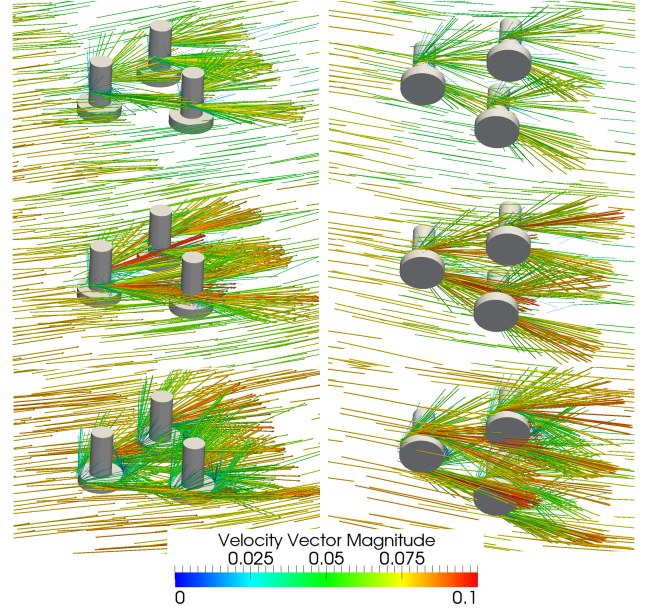


**FIGURE 13.** Velocity vectors at three depths below the free surface, 0.1, 0.2, and 0.3 m, from top to bottom respectively. The right column of images shows a view from an angle above, while the left column illustrates the view from an angle below the semisubmersible. The vectors are colored by magnitude.

giving the modified pressure,

$$\tilde{p} = p + \rho gz \quad (3)$$

where  $z$  is negative in the downward direction, hence the plus sign. The total pressure is many orders of magnitude larger than the modified pressure,  $\tilde{p}$ , term due to the dominance of the hydrostatics. However, the hydrostatic pressure varies only in the vertical direction ( $z$ ), such that  $\nabla p_x$  and  $\nabla p_y$  are dictated entirely by changes in the modified pressure. In this work, which focuses on drag loads, it is the changes in the  $x$ -direction of the pressure field that are of primary concern. Therefore, despite the dominance of the hydrostatics on the total pressure, variations in the modified pressure, specifically in the  $x$ -direction (current direction) are significant.

Isosurfaces of the modified pressure field,  $\tilde{p}$ , are shown in Figure 14. This image illustrates surfaces of constant pressure, without the contribution of the hydrostatic pressure. It is shown that lower pressure regions exist directly in front of the front column, and behind the trailing columns, as indicated by the dark blue pressure shell with a value of 3 Pa. The isosurfaces increase in magnitude inside of the three offset columns, most specifically on the front side of the trailing columns. This is shown with the red isosurface illustrating a pressure of 5.5 Pa. These variations in the modified pressure highlight the effects of the multicolumn

arrangement of the semisubmersible where the field appears to be directly affected by the presence of the downstream columns.

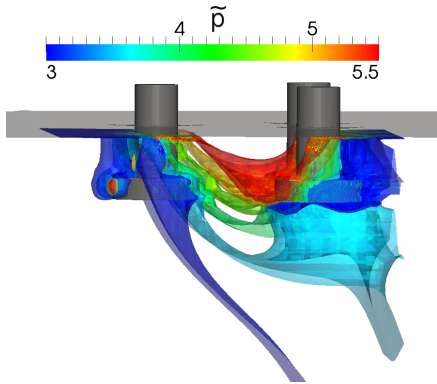


**FIGURE 14.** Isosurfaces of the modified pressure term,  $\bar{p}$ . A region of higher pressure is shown in between the three columns, which is believed to drive the flow downwards towards the trailing base columns.

The changes in the modified pressure term help to explain why the flow diverts downwards as it travels downstream, because the flow avoids the region of higher pressure that forms in between the three offset columns. The fluid motion is seen to move downwards after passing over the base column of the front pile. It then heads toward the base columns of the trailing columns with increased velocities, as is depicted in Figures 10 and 13. To further illustrate the increase in velocity, Figure 15 shows the magnitude of the velocity field mapped onto the pressure isosurfaces presented in Figure 14. Additionally, accelerations in the flow field are seen as the flow travels beneath the base columns, further explaining the increased drag on the base columns on the trailing columns and highlighting the role of the free ends of the structure.

The presence of a free surface, free ends and multibody arrangement is shown to play a role in the overall drag loading on the semisubmersible. A reduction in the velocity near the free surface as the flow approaches the body leads to overall lower drag coefficients on the upper columns. Flow accelerations beneath the structure, caused by the free ends, are shown to cause higher drag on the base columns in general. The multibody arrangement leads to increases in the fluid velocity coming off the front columns and heading downwards, causing increased drag on the base columns of the trailing piles. It is shown that the geometric differences between an infinitely long cylinder and the semisubmersible structure alter the drag predictions on the latter structure. These factors should be taken into consideration when selecting the most appropriate drag coefficients for input to engineering tools.

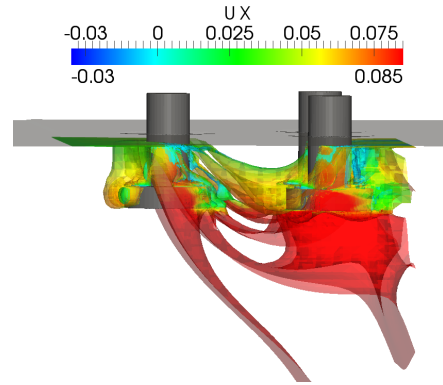


**FIGURE 15.** The x-component of velocity mapped onto the pressure isosurfaces illustrated in Figure 14.

### Isolated Offset Column

To better understand the effects of the multimember arrangement of the semisubmersible, a single, isolated offset column was simulated in 0.6 m/s current velocity. The resulting force predictions on the isolated offset column are compared against the loads on columns that are part of the multimember arrangement. Loads on the isolated column are presented here, alongside the predicted loads on the front and trailing columns discussed earlier.

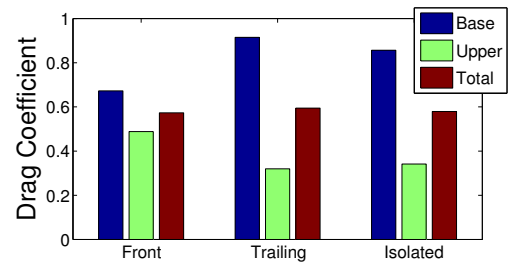


**FIGURE 16.** Drag coefficient predictions for the base column, upper column, and entire offset column for the front, trailing, and isolated columns of the semisubmersible.

The drag coefficients of the base column, upper column, and entire offset column, as predicted by CFD, are presented in Figure 16. The predicted drag coefficient for the base member of the isolated offset column falls between the predicted drag coefficients for the front and trailing columns' base members. The same trend exists for the upper member as well. This finding indicates that the presence of other members does alter the drag behavior on any one member.

### HydroDyn with Updated Drag Coefficients

The geometric complexities of the semisubmersible have demonstrated sizable effects on the drag behavior, as compared to that of an infinitely long cylinder. It may be the case that CFD simulations must be performed a priori to running simulations with engineering tools that use drag coefficients as inputs. To assess how far we can extend drag coefficients computed at a single current velocity, in this case at 0.6 m/s, the drag coefficients presented earlier were input to HydroDyn, and simulations were performed with current velocities of 0.3 and 1.0 m/s, for stationary semisubmersibles. The drag coefficients are given in Table 3, taken from Figure 9, and the results are presented here.

**TABLE 3.** Predicted drag coefficients from CFD, used as input to HydroDyn.

	Upper	Base
Front	0.488	0.673
Trailing Right	0.320	0.915
Trailing Left	0.322	0.922

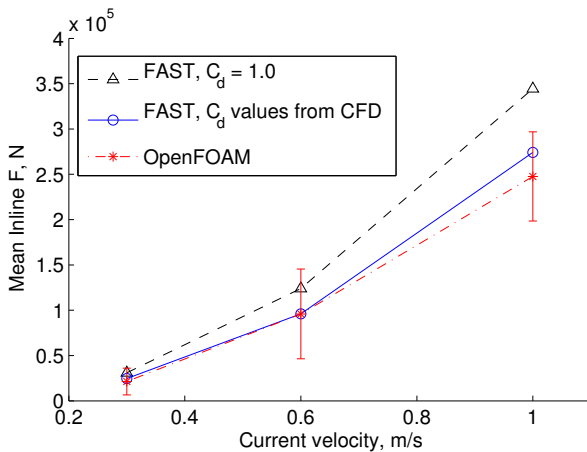


**FIGURE 17.** Comparison of mean in-line forces from OpenFOAM and FAST at three current velocities. FAST results when all members were assigned a drag coefficient of 1.0 are shown in black, while FAST results with drag coefficients from Table 3 are shown in blue. OpenFOAM results are given in red, where error bars indicated one standard deviation in the time-varying load.

The mean in-line force predictions from OpenFOAM at 0.3, 0.6, and 1.0 m/s current velocities are shown in Figure 17, alongside the load predictions from two sets of FAST simulations.

The first set of FAST simulations used drag coefficients of 1.0 for each member, while the second set of simulations used the drag coefficients listed in Table 3. As expected, the agreement between OpenFOAM and FAST is much better when the drag coefficient inputs to HydroDyn are taken from the CFD predictions. More importantly, the agreement improves for the 0.3 and 1.0 m/s current velocity cases, even when the drag coefficients are derived only from a 0.6 m/s case. This points to the ability to extrapolate drag coefficients computed from similar, but different, flow conditions.

### CONCLUSIONS

The drag behavior of the semisubmersible in current-only conditions was investigated with CFD simulations. The research presented here seeks to explain the code-to-code discrepancies seen in previous work between OpenFOAM and HydroDyn by investigating the combined effects of a free surface, a free end and the multiple member arrangement. This work demonstrates the large impact of these factors on the prediction load behavior, and argues that careful selection of input parameters for engineering tools is necessary.

Simulations were performed with OpenFOAM and HydroDyn for the case of the stationary semisubmersible in current-only conditions. The drag loads were compared quantitatively, and the results from CFD revealed drag coefficient predictions below the values for an infinitely long, fully submerged cylinder at the same Reynolds number. Flow visualizations from the CFD simulations were presented to explain the geometric factors leading to changes in the drag behavior. It was shown that the presence of a free surface as well as free ends leads to reductions in the drag coefficient as compared to infinitely long cylinders. Additionally, the multimember arrangement also lead to decreases in the drag loads.

HydroDyn, and other codes that use Morison’s equation, predict only mean forces. They do not capture time varying loads, which occur due to vortex shedding in both the inline and transverse flow directions. These oscillatory loads could have a significant impact on the fatigue of the semisubmersible and other similar offshore structures. The OpenFOAM results exhibit a very large variation in inline loads, as shown by the error bars in Figure 7.

The selection of drag coefficient for input to engineering tools should involve considerations of the presence of a free surface, free ends, and/or multimember arrangement. The drag behavior is altered significantly by these factors, such that the drag coefficient is much lower than that for an infinitely long, fully submerged cylinder at the same Reynolds number. Due to the sensitivity of the loads to these various factors, as well as the added complexity of their combined effects, it is likely necessary that CFD simulations be performed for each unique geometry to determine load coefficients. CFD grows increasingly expensive

with higher Reynolds numbers, making this task computationally demanding, but nonetheless beneficial. The model-scale  $Re$  is much smaller than the full-scale  $Re$ , and this mismatch in  $Re$  will be considered in the future.

Future work will also consider the fatigue implications of the time-varying loads not captured with HydroDyn, and other similar engineering tools. Additionally, simulations of the 6 degrees of freedom motion of the semisubmersible due to wave-body interactions will be performed. This future work will compare loading and motion predictions from OpenFOAM and HydroDyn for free decay tests, regular wave conditions, and extreme-load conditions in irregular waves.

## ACKNOWLEDGMENT

The authors would like to acknowledge the support of a grant from the Department of Energy, award number DE-AC36-08GO28308 as well as support from the Massachusetts Clean Energy Center. This work used the Extreme Science and Engineering Discovery Environment (XSEDE), which is supported by National Science Foundation grant number OCI-1053575. The authors acknowledge the Texas Advanced Computing Center (TACC) at The University of Texas at Austin for providing high performance computing resources that have contributed to the research results reported within this paper. <http://www.tacc.utexas.edu> for more information.

## REFERENCES

- [1] Jonkman, J., Robertson, A., and Hayman, G.J., 2014 “HydroDyn User’s Guide and Theory Manual,” National Renewable Energy Laboratory, Golden, CO.
- [2] Jonkman, J., and Buhl, M. L., 2006, “FAST User’s Guide,” NREL/EL-500-38230, National Renewable Energy Laboratory, Golden, CO.
- [3] Benitz, M.A., Schmidt, D.P., Lackner, M.A., Stewart, G.M., Jonkman, J. and Roberston, A., 2014, “Comparison of hydrodynamic load predictions between reduced order engineering models and computational fluid dynamics for the OC4-DeepCwind semisubmersible” *33rd International Conference on Ocean, Offshore and Arctic Engineering, San Francisco, CA, USA*.
- [4] Robertson, A., Jonkman, J., Masciola, M., Song, H., Goupee, A., Coulling, A., and Luan, C. “Definition of the Semisubmersible Floating System for Phase II of OC4,” Technical Report, NREL/TP-5000-60601. National Renewable Energy Laboratory, Golden, CO.
- [5] Chaplin, J.R. and Teigen, P., 2003, “Steady flow past a vertical surface-piercing circular cylinder” *Journal of Fluids and Structures* **18** pp. 271–285
- [6] Yu, G. and Avital, E.J. and Williams, J.J.R., 2008, “Large eddy simulation of flow past free surface piercing circular cylinders”, *ASME Journal of Fluids Engineering*, **130**
- [7] Kawamura, T. and Mayer, S. and Garapon, A. and Srensen, L., 2002, “Large eddy simulation of a flow past free surface piercing circular cylinder”, *ASME Journal of Fluids Engineering*, **124** pp. 91 –101
- [8] Suh, J.S. and Yang, J.M. and Stern, F., 2011, “The effect of air-water interface on the vortex shedding from a vertical circular cylinder”, *ASME Journal of Fluids Engineering*, **27** pp. 1–22.
- [9] Sumner, D. and Heseltine, J.L. and Dansereau, O.J.P., 2004, “Wake structure of a finite circular cylinder of small aspect ratio”, *Experiments in Fluids* **37** pp. 720 – 730
- [10] Niedzwecki, J. M. and Duggal, A.S., 1992, “Wave Runup and Forces on a Circular Cylinder in Regular and Random Waves,” *J. of Waterway, Port, Coastal, Ocean Eng.* **6**(118), pp. 615-620
- [11] Sumner, D., 2010, “Two circular cylinders in cross-flow: A review”, *Journal of Fluids and Structures*, **26** pp. 849–899
- [12] de Ridder, E. J., Koop, A. H., and van Doeveren, A. G., 2001, “DeepCwind Floating Wind Turbine Model Tests,” *Volume I. Report No. 24602-1-OB*, Wageningen, Netherlands.
- [13] Weller, H., Tabor, G., Jasak, H., and Fureby, C., 1998, “A Tensorial Approach to Computational Continuum Mechanics Using Object-oriented Techniques,” *Comput. Phys.*, **12** pp.620 - 631.
- [14] Noh, P. and Woodward, P., 1976, “SLIC (Simple Line Interface Calculation),” *5th International Conference on Fluid Dynamics*, 59.
- [15] Hirt, C.W. and B.D. Nichols, 1981, “Volume of fluid (VOF) method for the dynamics of free boundaries,” *J. Comp. Phys.*, **39** pp: 201–225.
- [16] DeBar, R., 1947, “Fundamentals of the KRAKEN Code,” *Technical Report, UCIR-760*, Lawrence Livermore National Lab, CA.
- [17] Rusche, H., 2002, “Computational Fluid Dynamics of Dispersed Two-Phase Flows at High Phase Fractions,” Imperial College of Science, Technology and Medicine, London.
- [18] Spalart, P. R., and Allmaras, S. R., 1992, “A One-Equation Turbulence Model for Aerodynamic Flows,” *American Institute of Aeronautics and Astronautics (AIAA) Paper 92-0439*, AIAA, Reston, VA.
- [19] Spalding, D. B., 1961, “A Single Formula for the Law of the Wall,” *Trans. ASME., J. Appl. Mech.* **28**(3) pp. 444-458.